Molecular Therapy
Original Article

# The neutralization effect of montelukast on SARS-CoV-2 is shown by multiscale *in silico* simulations and combined *in vitro* studies

Serdar Durdagi,[1] Timucin Avsar,[2] Muge Didem Orhan,[2] Muge Serhatli,[3] Bertan Koray Balcioglu,[3] Hasan Umit Ozturk,[3] Alisan Kayabolen,[4] Yuksel Cetin,[3] Seyma Aydinlik,[3] Tugba Bagci-Onder,[4,5] Saban Tekin,[3,6] Hasan Demirci,[7] Mustafa Guzel,[8] Atilla Akdemir,[9] Seyma Calis,[2,10] Lalehan Oktay,[1] Ilayda Tolu,[1] Yasar Enes Butun,[8] Ece Erdemoglu,[1,11] Alpsu Olkan,[1] Nurettin Tokay,[3] Şeyma Işık,[3] Aysenur Ozcan,[1,12] Elif Acar,[1,12] Sehriban Buyukkilic,[1,13] and Yesim Yumak[1,14]

[1]Department of Biophysics, Computational Biology and Molecular Simulations Laboratory, School of Medicine, Bahçeşehir University, Istanbul, Turkey; [2]Department of Medical Biology, School of Medicine, Bahçeşehir University, Istanbul, Turkey; [3]The Scientific and Technological Research Council of Turkey (TÜBİTAK) Marmara Research Center (MAM), Genetic Engineering and Biotechnology Institute, 41470 Gebze, Kocaeli; [4]Brain Cancer Research and Therapy Laboratory, Koç University School of Medicine, 34450 Istanbul, Turkey; [5]Koç University Research Center for Translational Medicine, 34450 Istanbul, Turkey; [6]Department of Basic Sciences, Division of Medical Biology, Faculty of Medicine, University of Health Sciences, Istanbul, Turkey; [7]Department of Molecular Biology and Genetics, Koç University, 34450 Istanbul, Turkey; [8]Department of Medical Pharmacology, International School of Medicine, Istanbul Medipol University, Istanbul, Turkey; [9]Department of Pharmacology, Computer-aided Drug Discovery Laboratory, Faculty of Pharmacy, Bezmialem Vakif University, Istanbul, Turkey; [10]Department of Molecular Biology-Genetics and Biotechnology, Istanbul Technical University, 34485 Istanbul, Turkey; [11]Faculty of Medicine, Mersin University, Mersin, Turkey; [12]Faculty of Medicine, Istanbul Medeniyet University, Istanbul, Turkey; [13]Faculty of Science, Necmettin Erbakan University, Konya, Turkey; [14]Faculty of Science and Letters, Tokat Gaziosmanpaşa University, Tokat, Turkey

**Small molecule inhibitors have previously been investigated in different studies as possible therapeutics in the treatment of severe acute respiratory syndrome coronavirus-2 (SARS-CoV-2). In the current drug repurposing study, we identified the leukotriene (D4) receptor antagonist montelukast as a novel agent that simultaneously targets two important drug targets of SARS-CoV-2. We initially demonstrated the dual inhibition profile of montelukast through multiscale molecular modeling studies. Next, we characterized its effect on both targets by different *in vitro* experiments including the enzyme (main protease) inhibition-based assay, surface plasmon resonance (SPR) spectroscopy, pseudovirus neutralization on HEK293T/hACE2+TMPRSS2, and virus neutralization assay using xCELLigence MP real-time cell analyzer. Our integrated *in silico* and *in vitro* results confirmed the dual potential effect of montelukast both on the main protease enzyme inhibition and virus entry into the host cell (spike/ACE2). The virus neutralization assay results showed that SARS-CoV-2 virus activity was delayed with montelukast for 20 h on the infected cells. The rapid use of new small molecules in the pandemic is very important today. Montelukast, whose pharmacokinetic and pharmacodynamic properties are very well characterized and has been widely used in the treatment of asthma since 1998, should urgently be completed in clinical phase studies and, if its effect is proved in clinical phase studies, it should be used against coronavirus disease 2019 (COVID-19).**

## INTRODUCTION

The 2019 new coronavirus (severe acute respiratory syndrome coronavirus-2 [SARS-CoV-2]), was first reported in December 2019 in Wuhan (Hubei, China). It has quickly spread to other countries all around the world and affected more than 215 million people worldwide, becoming an urgent global pandemic. Coronaviruses are enveloped, non-segmented, positive-sense RNA viruses belonging to the family of Coronaviridae, the largest family in Nidovirales and widely distributed in humans, other mammals, and birds, causing respiratory, enteric, hepatic, and neurological diseases. Seven species of coronavirus are known to cause disease in humans. Four of them (229E, OC43, NL63, and HKU1) are common and they mostly cause common cold symptoms in immunocompetent individuals, while the other three, SARS-CoV, Middle East respiratory syndrome coronavirus (MERS-CoV), and SARS-CoV-2, cause serious symptoms and death.[1] In addition to the common cold symptoms, SARS-CoV-2 shows many clinical signs, including severe pneumonia; clot formation; RNAemia; and increased incidence of endotheliitis, fatigue, and neurological and cardiac consequences.[2]

Received 21 April 2021; accepted 15 October 2021;
https://doi.org/10.1016/j.ymthe.2021.10.014.

**Correspondence:** Serdar Durdagi, Department of Biophysics, Computational Biology and Molecular Simulations Laboratory, School of Medicine, Bahçeşehir University, Istanbul, Turkey; Durdagi Research Group (DRG).
**E-mail:** serdar.durdagi@med.bau.edu.tr

All coronaviruses have specific genes in ORF1 downstream that encode proteins for viral replication and nucleocapsid and spike development.[3] SARS-CoV-2 has four structural proteins: nucleocapsid, envelope, membrane, and spike. These four proteins play a vital role during the viral infection.[4] The spike glycoprotein (S protein) located on the external surface of coronaviruses is responsible for the connection and entry of the virus to host cells.[1] The S protein mediates receptor recognition, cell attachment, and fusion during the viral infection. While the virus is in its natural environment, S protein of coronavirus is inactive. During viral infection, target cell proteases activate the S protein by cleaving it into S1 and S2 subunits, which are required to activate the membrane fusion domain after viral entry into target cells.[5] The S1 subunit includes the receptor binding domain (RBD). This domain binds directly to the peptidase domain of angiotensin converting enzyme 2 (ACE-2). S2 functions during membrane fusion.

The chymotrypsin-like cysteine protease called 3C-like protease (3CLpro), also called main protease (Mpro), in SARS-CoV-2 is a vital enzyme involved in processes such as the processing, assembly, and replication of the virus. Thus, Mpro is one of the ideal targets for drug design and development studies against SARS-CoV-2.[6]

One of the key characteristics of severe coronavirus disease 2019 (COVID-19) is increased cytokine production. It is thought that the severity of the disease is primarily associated with the cytokine storm, which is an aggressive immune response to the virus.[7] The number of white blood cells and neutrophils, and the levels of procalcitonin, C-reactive protein (CRP), and other inflammatory indices like interleukin (IL)-2, IL-7, IL-10, granulocyte-colony stimulating factor (GSCF), interferon inducible protein-10 (IP10), monocyte chemotactic protein-1 (MCP1), macrophage inflammatory protein-1α (MIP1A), and tumor necrosis factor (TNF), are significantly higher in severe cases in patients with COVID-19.[8,9] Specifically, IL-1β, IL-6, and IL-10 are the three most elevated cytokines in serious cases.[10,11] One result of the cytokine storm is lung injury that can develop into acute lung injury or its more severe type, which is known as acute respiratory distress syndrome (ARDS).

Studies have shown the relation between COVID-19 and the most common chronic conditions such as diabetes, cardiovascular diseases, respiratory system diseases, and immune system disorders.[7,12] Asthma and chronic obstructive pulmonary disease (COPD) are among the diseases of the respiratory system that are most emphasized. Asthma is a chronic inflammatory airway condition. There is significant evidence that represents the relation of asthmatic patients in the population with viral infections like rhinoviruses.[13–15] Virus infections causing upper respiratory tract infection, like influenza A, rhinovirus, and respiratory syncytial virus (RSV), elevate local leukotriene levels.[16] Leukotrienes, which play a role in the contraction of bronchial muscles, are effective in initiating and amplifying many biological responses, including mast cell cytokine secretion, macrophage activation, and dendritic cell maturation and migration. Leukotrienes (LTC4, LTD4, and LTE4), activated basophils, eosinophils, macrophages, and products of mast cells are types of lipids conjugated with peptides.[17]

LTD4 receptors belong to the G protein-coupled receptor (GPCR) family. Montelukast is a leukotriene (D4) receptor antagonist that is a member of the quinolines and it was approved by US Food and Drug Administration (FDA) as an oral tablet in 1998. It is a licensed drug used for allergic rhinitis, exercise-induced bronchospasm, and especially prophylaxis and chronic treatment of asthma. As a result of LTD4 blockage, nuclear factor kappa-B (NF-κB) pathway activation and release of the proinflammatory mediators (i.e., IL-6, -8, and -10; TNF-α; and MCP-1) decrease.[3] Considering these anti-inflammatory effects by leukotriene receptor inhibition and possible antiviral effects, montelukast may be considered as an effective medication against SARS-CoV-2.[18,19] Some studies claim that montelukast may play an immunomodulatory role as a leukotriene receptor inhibitor in treatment since one of the pathophysiological steps of severe COVID-19 cases is the cytokine storm resulting from excessive proinflammatory mediator release.[20,21]

Studies in the literature regarding the use of high doses (i.e., 200 mg/day) of montelukast show that its toxicity tolerance is high.[22] In the clinical study conducted by Altman et al.,[23] it was noted that at all doses (10 mg/day to 200 mg/day), montelukast had no significant clinical or laboratory side effects and was well tolerated at high doses. Three dose-interval studies (10, 100, 200 mg/day) were conducted to determine the optimal dosage of montelukast for oral administration.[22–24] The first of these randomized, double-blind, placebo-controlled studies examined the efficacy and safety of administered montelukast. It was administered once daily (10-, 100-, or 200-mg doses) or twice daily (10 or 50 mg) for 6 weeks to 343 chronic adult asthma patients with no serious side effects reported at high doses.[22–24]

Nowadays, the concept of drug repurposing is an evolving technique in which approved drugs are commonly used to identify potential candidates for different diseases. Developing new drugs from scratch is a long process and thus impractical to cope with the current global challenge.[25] Many drugs have several protein targets, and many diseases share molecular mechanisms that overlap each other. In this scenario, reusing drugs for new purposes and discovering their new uses by using computational approaches will dramatically lower the cost, time, and risks of the drug development processes.[26]

Here, initially we explored the potential role of montelukast in the management of SARS-CoV-2 infection with multiscale molecular modeling approaches. Computational analysis showed promising results both in the Mpro target and the spike/ACE2 interface. Moreover, the effect of the montelukast on SARS-CoV-2 variants emerging from the UK (B.1.1.7, also called alpha) South Africa (B.1.351, also called beta), and delta variant (B1.617.2) is also conducted with *in silico* simulations, and computational results confirm the effect of montelukast both on wild-type (WT) and mutant forms. Molecular modeling studies conducted for montelukast on SARS-CoV-2 targets encouraged us to perform further detailed *in vitro* experiments. The results of *in vitro* enzyme inhibition biochemical assays, surface plasmon resonance (SPR), pseudovirus neutralization, and virus

neutralization experiments demonstrated the significant effect of montelukast on SARS-CoV-2.

In one of our recent drug repurposing efforts,[27] we screened approved drugs and compounds in clinical phases at HIV-1 targets (protease and CCR5). Montelukast was among the proposed compounds, and this compound was purchased and added to our in-house small molecule library. A similar virtual drug repurposing approach was applied against SARS-CoV-2 targets when the COVID19 pandemic began, and montelukast was found to be a promising molecule in both the Mpro and the spike/ACE2 interface. Although there are many extensive and ongoing research studies to identify small therapeutics against COVID-19,[28–30] no effective small molecule-based therapy has yet been found. Therefore, the findings of this study may contribute to the discovery of new solutions for the treatment of this disease.

## RESULTS

### *In silico* drug repurposing studies suggest usage of montelukast against SARS-CoV-2

It has been recognized that the single-target, one-molecule approach is not very effective in treating complex diseases, and alternative combination drugs are not appreciated due to toxicity and/or unwanted drug-drug interactions.[27,31] The promising approach to these complex diseases is to develop single-multitarget compounds so that a molecule may interact with multiple related selected target proteins simultaneously. As new drugs are expensive and time consuming to develop, repositioning/reusing drugs has emerged as an alternative approach. Thus, in our recent study[27] we screened FDA-approved drugs and compounds in a clinical investigation to identify effective single-multitarget molecules against HIV-1. For this aim, two important and essential proteins in the HIV-1 life cycle, CCR5 co-receptor (belongs to the GPCR family) and HIV-1 protease (PR) enzyme, were targeted and about 25 potential hit compounds were identified. Montelukast was among the molecules we proposed as dual HIV-1 inhibitors with *in silico* simulations and that we purchased and added to our in-house small molecule library to evaluate *in silico* results. In our laboratory, *in silico*-guided screening and identification of the novel therapeutic hit compounds against different biological problems from FDA-approved drugs and compounds in clinical investigation or from large molecule libraries is one of the most important goals. We have built our in-house small molecule library from compounds we identified and purchased through simulations against different diseases. Therefore, we conducted a similar approach to identify potent inhibitors against SARS-CoV-2 from small molecule libraries. In this preliminary virtual screening study of our in-house small molecule library, which includes more than 150 approved drugs and compounds in clinical investigation phases, we achieved successful results for montelukast against SARS-CoV-2 Mpro and spike/ACE-2 targets. We therefore decided to carry it to further comprehensive *in silico* analyses.

Both noncovalent and covalent docking approaches are performed in the SARS-CoV-2 Mpro since recent structural biology studies show that the majority of the co-crystallized compounds at the Mpro construct bonded interactions.[32] Top-docking poses of montelukast were then used in micro-second-scale all-atom molecular dynamics (MD) simulations. Figure S1 shows representative structure of montelukast at the SARS-CoV-2 Mpro target obtained from saved trajectories throughout the MD simulations, which is initiated from noncovalent docking. Crucial residues in ligand interaction were found to be His41, Met49, Asn142, Met165, Glu166, Leu167, Pro168, Phe185, Gln189, and Ala191 (Figure S2). Corresponding interactions obtained from simulations initiated from covalent docking were Asn142, Gly143, Ser144, Cys145, His164, Glu166, and Gln189 (Figures 1 and S3).

The effect of montelukast on the SARS-CoV-2 spike/ACE-2 region was also investigated. The top-docking pose of montelukast at the spike/ACE-2 was used in the all-atom MD simulations. Figures 2 and S4 present 3D and 2D ligand interaction diagrams of montelukast at the spike/ACE2 interface, respectively. The important residues in ligand interactions are represented with histograms, and it was found that Lys26, Asp30, Val93, Pro389, Arg408, Lys417, Phe555, Asn556, and Arg559 are important residues that interact with the ligand.

The binding free energies of montelukast at the Mpro and spike/ACE2 targets were also investigated. Average molecular mechanics (MM) generalized Born surface area (GBSA) binding energy of montelukast at the binding cavity of Mpro was measured as $-79.60 \pm 8.66$ kcal/mol. When we increased the simulation time (i.e., simulations are increased by 3-fold), 3-μs simulations also showed that montelukast maintains its interactions with the crucial residues at the binding pocket of Mpro. Average MM/GBSA binding energy was calculated as $-84.86 \pm 9.22$ kcal/mol for 3-μs simulations. The corresponding average MM/GBSA value of montelukast at the spike/ACE-2 was calculated as $-43.93 \pm 7.66$ kcal/mol (Figure S5).

Furthermore, the effect of montelukast on the SARS-CoV-2 variants (i.e., alpha [B.1.1.7], beta [B.1.351], and delta [B.1.617.2]) are also considered. For this aim, we focused on Asn501Tyr, shared by both alpha and beta variants, and Lys417Asn and Glu484Lys mutations in the beta variant. Moreover, the effect of montelukast on the delta variant (B1.617.2) was also investigated. For this aim, Leu452Arg and Thr478Lys mutations were investigated. Single point mutations were performed in these residue regions and binding sites during the grid map generation were conducted both in WT and mutants in these regions (i.e., each grid map is formed from mentioned residue positions and, in order to compare with WT, grid maps are also formed at these regions individually for WT). Top-docking poses of montelukast at these regions were then used in MD simulations. Average MM/GBSA results showed that Asn501Tyr mutation, which is the common mutation in both variants, does not decrease the binding affinity of montelukast, and even more favorable (more negative) interaction energy at the mutant is observed by around 14% (Table S1). However, slight decrease in the binding affinity at the Lys417Asn and Glu484Lys mutation is observed (around %11 and around %4, respectively).

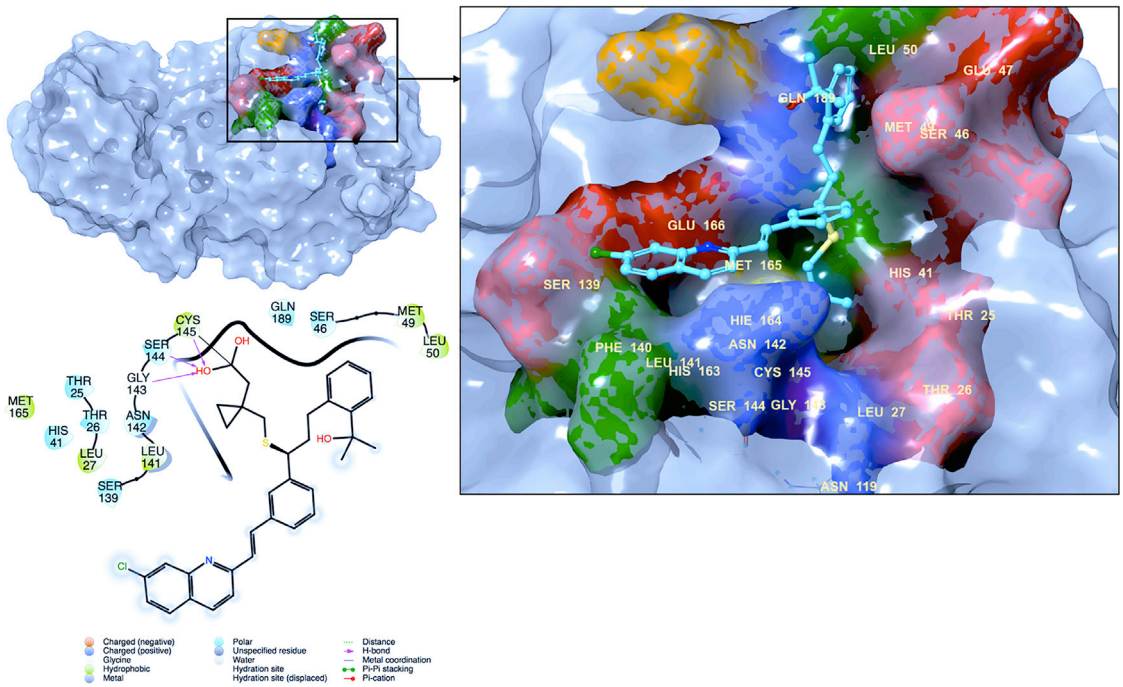


**Figure 1. Representative complex structure of montelukast at the binding pocket of the SARS-CoV-2 Mpro obtained from saved trajectories of MD simulations initiated with its covalent top-docking pose**

A 2D ligand interaction diagram is also shown.

Both in Leu452Arg and Thr478Lys mutations, more favorable interaction energies (more negative) with the ligand increased by about 20% and 8%, respectively. Thus, the comparison of average MM/GBSA results showed an effect of montelukast on both WT and variants (B.1.1.7, B.1.351, and B1.617.2) (Table S1).

### Mpro enzyme inhibition assay shows 74% loss of enzyme activity when using 100 μM montelukast

In this assay, the produced fluorescence due to the protease cleavage of the substrate was observed at 460 and 360 nm for emission and excitation wavelengths, respectively. The Mpro assay revealed that the montelukast molecule inhibits the Mpro enzyme activity in a concentration-dependent manner. The maximum inhibitory concentration was 100 μM and inhibited the enzyme activity by 74.04%. At 50 μM concentration inhibition, the enzyme activity was 60.59% (Figure 3). GC376 is a broad-spectrum antiviral that is used as a positive control molecule in the used assay and it showed 88.59% enzyme activity inhibition at 100 μM. Nonlinear regression analysis of five different concentrations revealed that 50% inhibition concentration ($IC_{50}$) of the montelukast molecule is 28.36 μM (Figure 3). Experiments are repeated at least six times in $IC_{50}$ measurement.

### The SPR assays demonstrate montelukast binding to SARS-CoV-2 Mpro

In the present study, together with SARS-CoV-2 Mpro enzyme inhibition analyses of montelukast, SPR spectroscopy was also used to evaluate the binding kinetics and affinity of this interaction. Biosensor technology from SPR has become an important tool for drug design and discovery. SPR techniques are used for a broad range of applications, including assessing the binding kinetics and affinity of an interaction, specificity tests, ligand screening, as well as analyte active binding concentration measurements. It can be used for the aim of drug screening for several diseases, including COVID-19. Here, SPR was used to estimate the potential role of montelukast in the management of SARS-CoV-2 infection and its binding kinetics on Mpro after analysis of multiscale molecular modeling studies and Mpro enzyme inhibition assays.

Solvent correction for 9.2% DMSO is shown in Figure 3. The affinity of montelukast for immobilized Mpro was determined using a 1:1 steady-state binding affinity interaction model. A concentration series ranging from 900 μM to 11 μM (in 3-fold dilutions) was injected over immobilized Mpro for 60 s followed by a 120-s dissociation phase. The responses obtained from each montelukast concentration were plotted against concentration using the Biacore T200 evaluation software and were evaluated using a 1:1 steady-state binding model. Montelukast was identified as a specific binder to Mpro (Figures 4 and S6). Its $K_D$ value was measured as 23.5 μM, which fits well with the $IC_{50}$ value determined by the 3CL enzyme inhibition assay (Figure 4). The observed concentration-dependent binding responses from the preliminary results indicate that the montelukast molecule interacts with Mpro with an affinity in the micro-molar range. According to the sensorgrams, the interactions do not reach a plateau (equilibrium phase) and also the small decrease of the sensorgrams

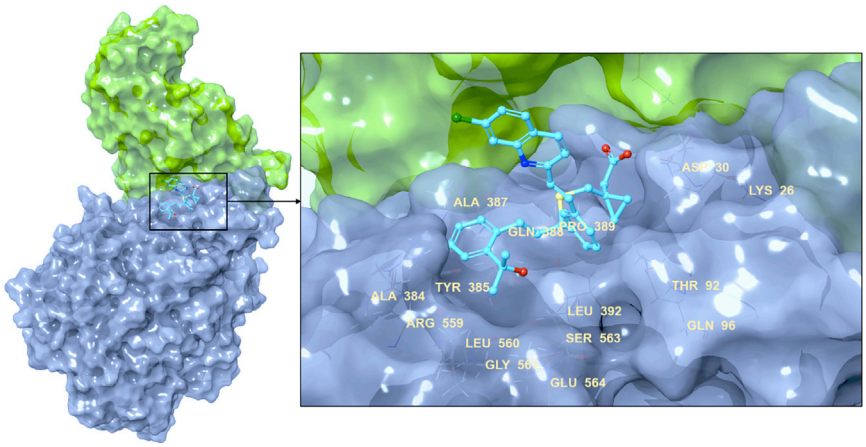


**Figure 2. Representative complex structure of montelukast at the SARS-CoV-2 spike/ACE-2 interface obtained from saved trajectories of MD simulations initiated with its noncovalent top-docking pose**

at the end of the binding phase indicate that some aggregation issue might be present. Therefore, the determination of the exact binding affinity constant of the montelukast to Mpro is restrained.

The square shape of sensorgrams shows that both montelukast binding to Mpro and complex dissociation are fast processes. This kind of binding behavior is, however, relatively common for small molecules.

### Neutralization potential of montelukast against SARS-CoV-2 was confirmed by pseudovirus neutralization on HEK293T/hACE2+TMPRSS2 cells

Pseudoviruses are useful tools (especially for emerging and re-emerging viruses) due to their safety and versatility. To increase the transfection and infection potency in the development stage of the pseudovirus, the main factors, including selection of plasmids, cell types, cell numbers, and virus inoculum, need to be optimized. In this study, pseudovirus neutralization assay was developed for screening the computationally selected drug, montelukast, as a potent inhibitor of SARS-CoV-2 spike-mediated cell entry.

#### *Cell viability*

To investigate the dose-response relationship of montelukast using the cell lines of HEK293T, Vero E6, Calu-3, and A549, the cell viability was measured upon 24-, 48-, and 72-h exposure periods by 3-[4,5-dimethylthiazol-2-yl]-2,5- diphenyltetrazolium bromide (MTT) calorimetric assay. As shown in Figure S7, the HEK293T cell monolayer was found to be the most sensitive cell line across the montelukast exposure, followed by Vero E6, A549, and Calu-3. The $IC_{50}$ value of montelukast toward the used cell lines after 24-, 48-, and 72-h exposure periods are given in Table 1. The result of the cell viability assay allows us to determine the concentration ranges for the pseudovirus neutralization assay.

#### *Pseudovirus neutralization*

Pseudovirus neutralization on HEK293T/hACE2+TMPRSS2 cells was performed using montelukast at the concentration ranges of 1–50 μM (Figure 5). We preferred to use HEK293T cell lines, which have a transient ACE2 and TMPRSS2 expression. To evaluate antiviral measures for SARS-CoV-2, the pseudovirus neutralization assay would be used to evaluate inhibition of viral attachment and entry mediated by S protein screening.[31]

In our study, the pseudovirus neutralization test was performed in three different ways to test montelukast binding to the spike/ACE2 interface: (1) [montelukast + pseudovirus]cell; (ii) [cell + montelukast]pseudovirus; (iii) [cell + pseudovirus]montelukast. The 50% effective pseudovirus neutralization drug doses ($EC_{50}$) were found to be 48.98 μM for [pseudovirus + cell]montelukast, >50 μM for [cell + montelukast]pseudovirus, and 43.79 μM for [pseudovirus + montelukast]cell treatments, whereas the cell viability was in the range of 86%–90% at these concentrations. A similar neutralization trend among the treatments was seen as obtained from the xCELLigence assay. The [pseudovirus + montelukast] cell treatment resulted in the most effective neutralization, as expected, since it allows binding of the drug to spike proteins around the pseudovirus before the cell treatment. This can be interpreted as an indicator of montelukast binding to the spike/ACE2 interface.

Moreover, to evaluate the neutralization potential of different SARS-CoV-2 variants by montelukast, SARS-CoV-2 S pseudovirion WT, alpha, and beta variants' neutralization on HEK293T/hACE2+-TMPRSS2 by montelukast was investigated. Inhibition of alpha and beta pseudovirus variants' entry to the HEK293T/hACE2+TMPRSS2 cells via montelukast was observed to increase in a dose-dependent manner, similar to the WT (Figure S8). To evaluate the cell viability at the same concentrations as were used for neutralization, the luciferase activity was measured 72 h post transduction by CellTiter-Glo Luminescent Cell Viability Assay Kit (Figure 5A). The entry efficiency of SARS-CoV-2 pseudoviruses without any treatment was taken as 100%. The representative cell viability and infection at different concentrations are shown in the images taken with 10× magnification during the neutralization period (Figure 5B).

### Virus neutralization assay using xCELLigence MP real-time cell analyzer demonstrates the effective virus neutralization concentration of montelukast

Neutralization assay was performed based on impedance using xCELLigence MP real-time cell analyzer (RTCA) equipment. In this work, VERO E6 cells were used (ATCC CRL 1586). The impedance is expressed as arbitrary units called cell index (CI). Data were collected for 130 h with intervals of 15 min.[33–36]

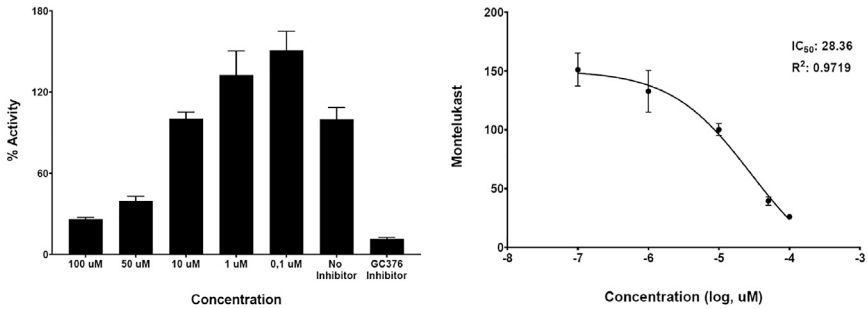


**Figure 3. (left) 3CL Protease activity in the presence of montelukast with ranging concentrations**

Inhibitory activity is the inhibited 3CL (Mpro) enzyme activity percentage. "No Inhibitor" represents the 3CL protease activity without any inhibitors, and GC376 inhibitor is a broad-spectrum antiviral used for comparison. (Right) Dose-response curve of montelukast against 3CL protease. Experiments are repeated at least three times.

Three different experiments were designed to investigate the effect of the montelukast against the SARS-CoV-2. First, montelukast was incubated 1 h before the cell was infected with the virus, i.e., [montelukast + cell]virus. Therefore, an attempt was made to imitate the infection in the early period to investigate the protective effect of the montelukast. Second, cells were infected with virus and then montelukast was added i.e., [cell + virus]montelukast. Thus, the effectiveness of the drug was investigated in the late phase. As a final experiment, montelukast was interacted with the virus, then added to the medium, i.e., [montelukast + virus]cell. This last sampling was done to see if the drug has a protective effect against the virus. With those three different methods, the effective concentration on the SARS-CoV-2 was found to be 25 μM (Figure S9).

The cell index time 50 ($CIT_{50}$) is the time required for the CI to decrease by 50% after virus infection.[37] In the different methods tested, when the $CIT_{50}$ values of the most effective dose are compared, the second method ([cell + virus]montelukast) shown as stands out with 20-h delay of viral effects. The first method ([montelukast + cell]virus) and a third method ([montelukast + virus]cell) were followed with 8 and 13 h of delay, respectively (Figure 6).

## DISCUSSION

Here, the potential effect of montelukast on SARS-CoV-2 is investigated using multiscale molecular modeling approaches and integrated *in vitro* experiments, including 3CL enzyme inhibition-based binding assays, SPR, pseudovirus, and virus neutralization methods. Hypotheses and *in silico* studies regarding the use of montelukast against COVID-19 have been discussed in the literature.[18,38,39] While most of these reports are limited to only hypotheses, some studies have emphasized only *in silico* results.[40–42] For example, Copertino et al.[42] hypothesized that since montelukast had previously been shown to have antiviral activity against Zika and dengue viruses as well as because of its immune modulatory profiles, it may be considered for biological activity against COVID-19. In our study, for the first time in the literature, combined multiscale molecular modeling studies and different *in vitro* experiments were conducted to better understand the effect of montelukast on SARS-CoV-2.

Our results show that montelukast has a dual inhibitor effect and exerts its effect on SARS-CoV-2 by interference with the entry of the virus into the host cell (via spike/ACE-2) as well as inhibiting the 3C-like protease, which is responsible for functional protein maturation. Our computational results also showed the effect of montelukast on the alpha, beta, and delta variants, and its effect on alpha and beta variants was also confirmed by pseudovirus neutralization assays. Thus, in the current study, our integrated *in silico* and combined *in vitro* experiments show the effect of montelukast on SARS-CoV-2.

As was confirmed from both the pseudovirus and virus neutralization assays, the most likely clinical use of montelukast after infection of SARS-CoV-2 ([pseudovirus + cell]montelukast treatment) was the effective neutralization of virus.

Our virus neutralization assay results show that montelukast with 25 μM concentration delayed the effect of virus for 20 h when cells were infected with virus and then montelukast was added; i.e., [cell + virus]montelukast. In other methods, such as when montelukast was incubated within 1 h before the cell was infected with the virus, the delay time was found to be 8 h. Therefore, montelukast might also be considered for its prophylactic effect.

We described a detailed procedure of pseudovirus neutralization assay for SARS-CoV-2 using a HEK293T cell expressing ACE2 and TMPRSS2. On the other hand, we performed a neutralization assay based on impedance using xCELLigence MP RTCA equipment. We realized that Vero E6 cells were first used as target cells for neutralization assays in the literature; however, we observed that they were relatively insensitive to pseudovirus at certain plaque-forming units (PFUs) compared with HEK293T cells expressing ACE2 and TMPRSS2. Neerukonda et al. found that the Vero E6 cells and HEK293T cell line, which does not express ACE2 and TMPRSS2, showed low transduction efficiency against SARS-CoV-2 pseudoviruses. It has been claimed that the major reason for the Vero E6 cell showing that pseudovirus lacked infectivity is its resistance to human lentivirus infection due to intrinsic restriction factors.[43] In another study, transduction efficiencies of HEK293T, HeLa-P4, and Vero E6 cells were compared against HIV-1-derived lentiviral vectors, and high transduction efficiencies of HEK293T and HeLa-P4 were found compared with Vero E6 cells.[44] Moreover, HEK293FT cells expressing both ACE2 and TMPRSS2 and Vero E6 cells were infected with the highest average titer of D614G R682G Δ19 spike pseudovirus, and higher infectivity was found in HEK293FT cells (ACE2+ TMPRSS2+) compared with Vero E6 cells due to resistance to HIV-1

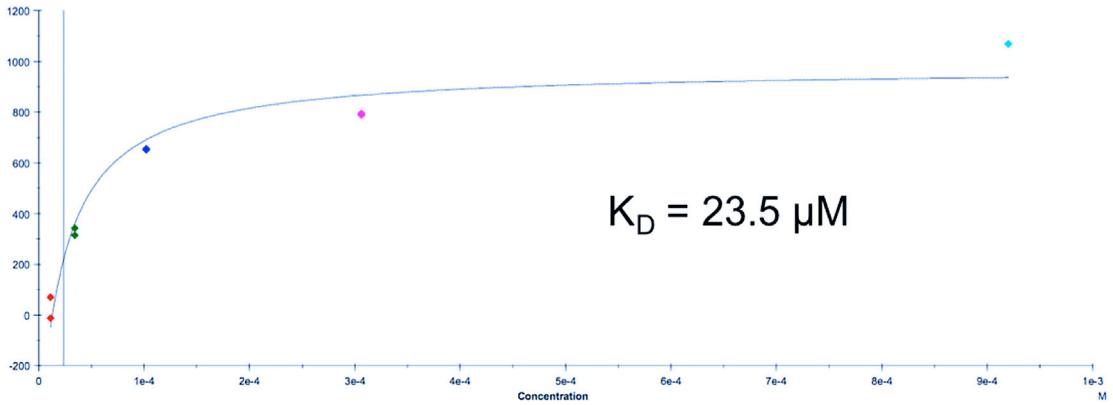


**Figure 4. Subtracted and correction sensograms of montelukast binding curves for 3C-like protease**

lentivirus infection.[45] On the other hand, Xiong et al. showed that the difference in infection efficiency between the VSVdG pseudotyped with full-length SARS-CoV-2 S protein or truncated SARS-CoV-2 Sdel18 protein with C-terminal 18 amino acid (aa) truncation and compared the infection efficiency of pseudotypes in Vero-E6, BHK21, BHK21-hACE2, and HEK293T cells.[46] Accordingly, Vero-E6 and BHK21-hACE2s cells were most sensitive to VSVdG-SARS-CoV-2- Sdel18 packaged pseudovirus infection compared with HEK293T and BHK21 cells.[46] Hence, these studies demonstrated that a selection of a cell line and a pseudovirus system that is most appropriate for pseudotype production and infection is an important step for pseudotyped neutralization assays. Since Vero E6 cells express a high level of ACE2 and are widely preferred for SARS-CoV-2 research, we used Vero E6 cells to investigate montelukast neutralization potential in live SARS-CoV-2 infection in our study. However, for pseudovirus neutralization assay, we preferred to use HEK293T cell lines, which have a transient ACE2 and TMPRSS2 expression.

Moreover, HEK293T cells, which transiently express both ACE2 and TMPRSS2t, supported the highest levels of infectivity for pseudoviruses. Johnson et al. reported that stable introduction of the spike-activating protease TMPRSS2 further enhanced susceptibility to infection by 5- to 10-fold.[45]

Kumar et al.[47] assessed the activity of montelukast using an *in vitro* cell culture model of SARS-CoV2 in VeroE6 cells, and the $IC_{50}$ of montelukast was measured as 18.82 µM, which fits well with our results.

Significant efficacy of montelukast against COVID-19 has been demonstrated in our study by hybrid *in silico* and different *in vitro* tests, but a limitation of the study is that these results have not yet been demonstrated by *in vivo* studies.

Since montelukast is an approved drug and has been widely used in the market for over 20 years against asthma, its side effects have been well studied and the results show that it is a well-tolerated drug even at very high doses (>200 mg/day). Since its patent expired in 2012, its clinical usage for COVID-19 can be urgently considered. Thus, phase-II clinical studies of montelukast by our group[32] have also been initiated in nine different centers in Turkey (clinicaltrials.gov, NCT04718285).

## MATERIALS AND METHODS

### Molecular modeling studies

Before the molecular docking and MD simulations, both ligand structure and used target protein structures were prepared. Montelukast structure was downloaded from PubChem (https://pubchem.ncbi.nlm.nih.gov/) and LigPrep module of the Maestro molecular modeling package was used in ligand preparation with OPLS3e force field. Epik was used in the determination of the protonation states at neutral pH.[48] While the crystal structure of Mpro, which was recently solved by our research group (PDB: 7CWB) at near-physiological temperature,[32] was used in docking and MD simulations, the 6M0J PDB-coded structure was used in drug docking and all-atom MD simulations for the spike/ACE-2 region. The protein preparation tool of Maestro was used in both targets at physiological pH. Bond orders are assigned, and hydrogens were added. Disulfide bonds were created, and missing side chains were fixed using Prime.[49] Water molecules beyond 5 Å from hetero groups were removed. PROPKA was used in the protonation states of the residues. OPLS3e force field was used in the restraint minimization with heavy atom convergence of 0.3 Å.

### Noncovalent docking

The prepared target proteins and ligand structure were used for molecular docking simulations. We performed a grid-based docking method (Glide/SP) at the docking.[50] The binding site of the Mpro was defined by centering grids at the centroid of a set of three crucial residues in ligand binding, namely His41, Cys145, and Glu166. Ali and Vijayan[51] described very strong and sustained salt bridge interactions between Lys417 of SARS-CoV-2 spike RBD and Asp30 of ACE-2. Thus, the corresponding residues at the spike/ACE-2 were used in grid generation. Top-docking poses obtained from noncovalent docking are used in all-atom MD simulations. For the SARS-CoV-2 spike mutation studies, grid maps are generated from three different points (from Asn501 for WT and N501Y mutant, from K417 for WT and K417N mutant, and from E484 for WT and E484K mutant structures).

**Table 1. The $IC_{50}$ values of montelukast toward the used HEK293T, Vero E6, Calu-3, and A549 cells lines obtained from dose-response curves**

| $IC_{50}$ values of montelukast (μM) | | | | |
|---|---|---|---|---|
| Exposure (h) | HEK293T | Vero E6 | Calu-3 | A549 |
| 24 | 92.2 ± 0.8 | 92.39 ± 3.8 | 72.7 ± 0.3 | 117.6 ± 1.4 |
| 48 | 35.3 ± 4.0 | 38.80 ± 2.5 | 47.1 ± 1.3 | 38.2 ± 1.9 |
| 72 | 23.0 ± 0.8 | 28.11 ± 3.1 | 50.7 ± 1.9 | 38.5 ± 0.8 |

Mean ± SD values were calculated from three independent experiments carried out in triplicate.

### Covalent docking

When the ligand forms a covalent bond with a binding pocket residue, the binding energy of the ligand is not only from the construction of a covalent bond but also from stabilizing nonbonding interactions. Here, we used a covalent docking module from Maestro, which selects the top-covalent bond poses using the Prime energy model.[52] In this method, docking starts with Glide docking with the reactive residue trimmed to alanine residue. The reactive residue of the target protein is then added and sampled to form a covalent bond with the ligand in different poses. Formed poses with covalent bond are minimized using the Prime VSGB2.0 energy model to score the top-covalent poses. In covalent docking, the ligand binding site was detected from three crucial residues at the Mpro, namely His41, Cys145, and Glu166. As the reaction type, the "nucleophilic addition to a double bond" option is selected with the guidance of the covalent bonded co-crystalized structures of inhibitors at the Mpro. In the docking process, default parameters were used.

### MD simulations and MM/GBSA analyses

The selected docking poses of montelukast at the Mpro and spike/ACE-2 targets were used in MD simulations. The used top-docking poses of complex structures were placed in simulation boxes with orthorhombic box (box size was calculated based on buffer distance of 10.0 Å) and solvated with TIP3P water models. The simulation systems were neutralized by the addition of counter ions, and a 0.15 M NaCl solution was used. Desmond program was used for all-atom MD simulations.[53] Before the production run, the systems were equilibrated using the default relaxation protocol of the Desmond. Simulations were performed at constant physiological temperature (310 K) and constant pressure (1.01325 bar). For this aim, NPT ensemble was used with Nose-Hoover thermostat[54,55] and Martyna-Tobias-Klein barostat.[56] Smooth particle mesh Ewald method[57] was used to calculate long-range electrostatic interactions with periodic boundary conditions. The cutoff distance was set to 9.0 Å for short-range electrostatics and Lennard-Jones interactions. The RESPA multi-step integrator was used. The time steps were varied for interaction types (bonded and near, 2 fs; far, 6 fs). Production time of the simulation was up to 3 μs for Mpro and 0.5 μs for spike/ACE-2 simulations. In the spike/ACE2 target protein (PDB: 6M0J), glycans were included at the simulations. The OPLS3e force field was used in simulations.[58] Two-thousand trajectory frames were recorded with equal intervals during the simulations. The average MM/GBSA binding free energy of montelukast was calculated for 200 trajectory frames throughout the simulations. The VSGB 2.0 solvation model was utilized during MM/GBSA calculations.

### The 3CL Protease enzyme inhibition assay

*In vitro* enzyme inhibition assays were carried out using SARS-CoV-2 3CL Protease assay kit (#79955-1 and #79955-2, BPS Bioscience, San Diego CA) and in accordance with manufacturer's protocol. A 100 mM stock concentration of montelukast was solved with dimethyl sulfoxide (DMSO), then diluted to working concentrations ranging from 100 nM to 100 μM with 1× assay buffer (20 mM Tris, 100 mM NaCl, 1 mM EDTA, 1 mM DTT, pH 7.3) as the manufacturer suggested. Final DMSO concentrations were below 1% for each tested concentration. Fifteen microliters of 3CL Protease enzyme was distributed to each well except blanks. GC376 was used as an inhibitor control. Five microliters of GC376 (50 μM) was added to the wells designated as inhibitor control. Five microliters of inhibitor in different concentrations (100 nM, 10 nM, 1 nM, 1 μM, 10 μM, 100 μM) was added to their relative wells, and a 1× assay buffer/DMSO mixture was added to blanks and positive controls. Two-hundred and fifty micromolar 3CL protease substrate was added to each well to start the reaction, and its final concentration was 50 μM in 25-μL volume. After 4 h of incubation at room temperature (RT), fluorescence was measured by a microtiter plate reader (Hidex Sense multi-mode reader, Finland) at a wavelength of 360 nm for excitation and 460 nm for emission. Blank values are subtracted from values of all other wells. Percentage inhibitory activity of each concentration were calculated, the fluorescence value from GC376 inhibitor control was set as 0% activity, and the fluorescence value from no inhibitor control was set as 100% activity. The $IC_{50}$ value was also determined by 3CL inhibitory screening assay. Absorbance values were recorded and the corresponding $IC_{50}$ value was calculated by dose-response inhibition curve and nonlinear regression analysis. The results were plotted with GraphPad Prism 8.0 software (GraphPad, San Diego CA).

### SPR

A Biacore T200 spectrometer Cytiva (Uppsala, Sweden) instrument was used. 3C-like proteinase (Mybiosource), Biacore Amine Coupling Kit (Cytiva), Series S Sensor Chip CM5 (Cytiva), and phosphate-buffered saline (PBS) containing 9.2% DMSO at pH 7.4 was used as running buffer.

#### *Immobilization pH scouting*

The best immobilization condition for Mpro on CM5 chip was determined by scouting of a 10 mM sodium acetate buffer at three different pH values: pH 4.0, 4.5, and 5.0. We determined that pH 4.0 was the optimal pH for immobilization.

#### *Surface preparation with immobilization of Mpro*

Mpro was immobilized on CM5 Sensor Chip by activating the surface with 0.4 mol/L EDC/0.1 mol/L N-hydroxysuccinimide (NHS) at a flow rate of 30 μL/min for 7 min. Mpro was dissolved in a 10 mM sodium acetate buffer, pH 4.0, to yield a 30-μg/mL solution. Following activation, Mpro solution was injected over the activated sensor chip surface at a flow rate of 30 μL/min for 6 min. Final ligand (Mpro)

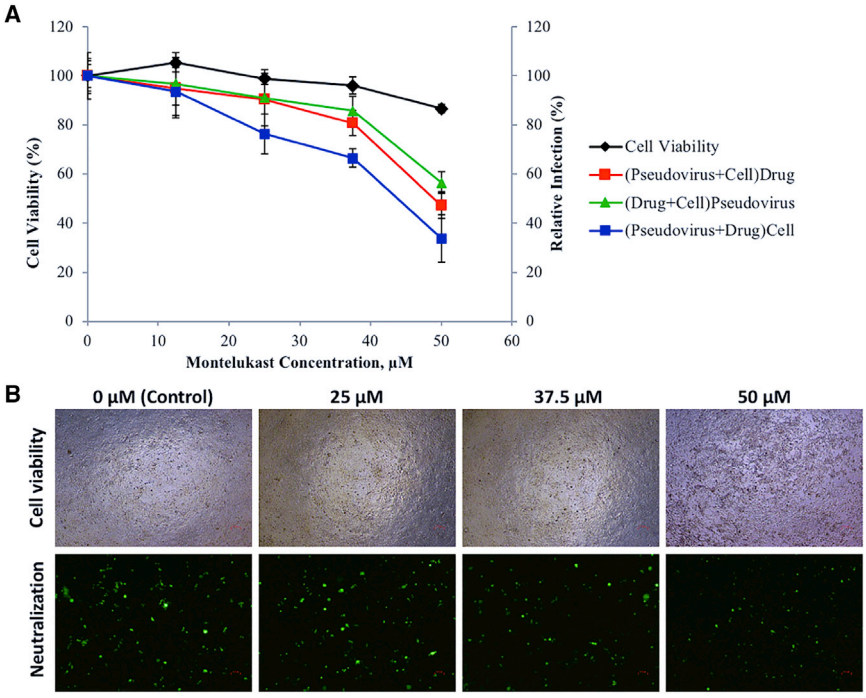


**Figure 5. Pseudovirus neutralization on HEK293T/hACE2+TMPRSS2 cells by montelukast**

(A) Effects of montelukast on the entry of pseudoviruses into HEK293T/hACE2+TMPRSS2 cells were examined in three ways: (1) the cell + pseudovirus was pretreated for 1 h at 37°C and then drug was added, (2) the cell + drug was pretreated for 1 h at 37°C and then pseudovirus was added, (3) the drug + pseudovirus was pretreated for 1 h at 37°C and then added to the cells. The fluorescence and luminescence levels were measured 72 h post transduction. The entry efficiency of SARS-CoV-2 pseudoviruses without any treatment was taken as 100%. Each dose was tested in triplicate and error bars indicate SEM of triplicates. (B) The representative images for the cell viability and neutralization were shown upon neutralization period, 72 h. Magnification 10×.

immobilization levels achieved were 11,330 response units (RUs). The excess hydroxysuccinimidyl on the surface was deactivated with 1 M ethanolamine hydrochloride, pH 8.5, for 7 min at a flow rate of 30 μL/min. The surface of a reference flow cell was activated with 0.4 mol/L EDC/0.1 mol/L NHS and then deactivated with 1 mol/L ethanolamine, with respective flow rates and times.

#### *Analyte injection*

Before analyte injection, the sensor chip surface was conditioned with three 12.5 mM NaOH pulses of 30 s followed by three start-up cycles, allowing the response to stabilize before analyte injection. We used eight different percentages of DMSO solutions (10.0%, 9.8%, 9.6%, 9.4%, 9.2%, 9.0%, 8.8%, and 8.6%) in the solvent correction cycles to correct responses for variations in the bulk refractive index of the samples. Data were collected at a temperature of 25°C and a 1-Hz rate. Montelukast was tested from lowest to highest concentration. During each sample cycle, analyte was injected for 60 s at a flow rate of 30 μL/min. Dissociation period was monitored for 120 s after analyte injection before regeneration with 12.5 mM NaOH for 30 s at a flow rate of 30 μL/min to wash any remaining analyte from the sensor chip and wash flow with 50% DMSO before running the next sample.

#### *1:1 steady-state binding affinity analysis*

Responses measured in the blank flow cell (control) were subtracted from the response measured in the active flow cell. The binding affinity ($K_D$) of the interaction was obtained by plotting double-referenced binding responses versus montelukast concentration and fitting the curve using a 1:1 steady-state affinity with constant $R_{max}$ interaction model.

### Cell viability assay

#### *Cell culture conditions*

The human embryonic kidney (HEK293T CRL-11268) and *Cercopithecus aethiops* kidney (Vero E6, CRL1586), human lung adenocarcinoma (Calu-3, HTB-55; A549, CCL185) cell lines were purchased from American Type Culture Collection (ATCC, United States). They were cultured in Dulbecco's Modified Eagle Medium (DMEM, p# 41965 Gibco) including 10% fetal bovine serum (FBS; p# 10,500 Gibco), 1% antibiotic-antimycotic in the tissue flasks, and incubated at 37°C and 5% $CO_2$. They were subcultured and used for cell viability and pseudovirus neutralization assay when they reach 70%–80% confluency.

#### *Cell viability assay*

HEK293T, Vero E6, Calu-3, and A549 cells were cultured at a cell density of $1 \times 10^4$ in the 96-well plates incubated at 37°C, and 5% CO2 for 24 h. The following day, after aspiration of the medium, montelukast (p# 1446859 Sigma-Aldrich) was added at concentrations of 1, 5, 10, 25, 50, 100, and 200 μM in DMEM and incubated for 24, 48, and 72 h. To measure the cell viability, MTT (p# M5655, Sigma-Aldrich) was dissolved in PBS, 5 mg/mL). After each incubation periods, MTT at 5 μg/mL in DMEM was added into the each well and incubated at 37°C and 5% $CO_2$ for 4 h. The formazan crystal-dissolving solution, dimethyl sulfoxide (DMSO, p# D 8418, Sigma-Aldrich) was added into each well and incubated for 2 h. The absorbance was measured on an ELISA plate reader with a test wavelength of 570 nm and a reference wavelength of 630 nm.

### Pseudovirus production and infection

#### *Transfection*

HEK293T is a highly transfectable cell line and widely used for retroviral production. Lentiviral-based pseudoviruses bearing SARS-CoV-2 S and its alpha and beta variants or VSV-G glycoproteins were produced based on previous studies.[59] Briefly, HEK293T cells were seeded at a cell density of $5 \times 10^5$ cells/well on the six-well plates. Next day, the cells in each well at approximately 70%–80% confluency were used for

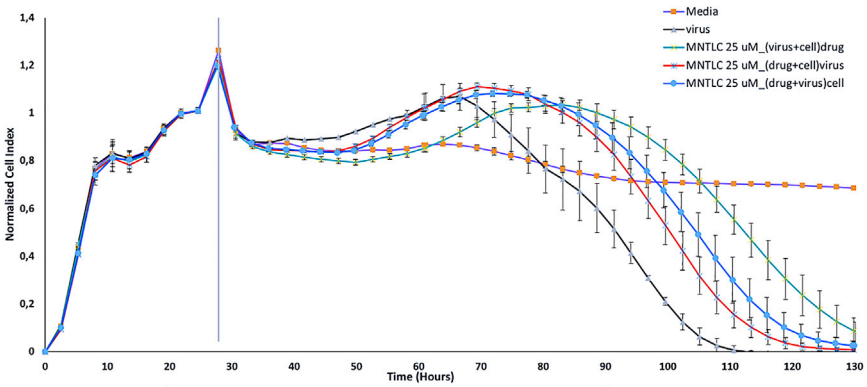


| Sample 25 uM | CIT50 (Hours) |
|---|---|
| Virus (SARS-CoV-2) | 92 |
| (Drug+Cell @37C 1h)Virus | 100 |
| (Drug+Virus @37C 1h)Cell | 105 |
| (Cell+Virus @37C 1h)Drug | 112 |

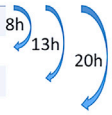


**Figure 6. Real-time cell analysis result of montelukast**

Data were collected for 130 h with intervals of 15 min. In the different methods tested and within those three methods, the effective concentration on the SARS-CoV-2 virus was found to be 25 μM. At the end of the period, the experiment was terminated, and the data obtained were analyzed using RTCA Software Pro software. $CIT_{50}$ values are presented for comparison, and the method, depicted as (cell + virus)Drug, becomes prominent, with 20 h of retention of the viral effects.

transfection. After aspiration of the medium from each well, the transfection agent Fugene-6 in 10 μL was added to the 100 μL of DMEM basal medium (without FBS and penicillin/streptomycin [Pen/Strep]) in the 1.5-mL tube and incubated for 5 min at RT. In another tube, 7,500 ng of lenti RRL_GFP reporter plasmid, 6,750 ng of psPAX2 packaging plasmid (Addgene plasmid # 12260), and 750 ng of spike-18aa truncated (Addgene plasmid # 149541)/its alpha variant/its beta variant was mixed. The plasmid mix was added into the fugen-6 tube and incubated for 25–30 min at RT and then placed drop by drop over the cells in the well. After 14–16 h of transfection, the medium was removed, and fresh full medium (DMEM with 10% FBS and 1% Pen/Strep) was added on the cells. After 48 h of transfection, WT, alpha, and beta variants of the pseudoviruses were collected, filtered through 0.45-μm syringe filters, and stored at +4°C for short-term usage (up to 3–4 days), or stored at −80°C for long-term storage.

Alpha and beta variants of pseudoviruses were produced by site-directed mutagenesis using Q5 site-directed mutagenesis kit (NEB), according to manufacturer's instructions. To construct alpha variant, H69V70 deletion and N501Y, D614G, P681H substitutions were performed on spike-18aa plasmid. On the other hand, K417N, E484K, N501Y, and D614G substitutions were performed on the spike-18aa plasmid to construct the beta variant.

### Pseudovirus neutralization assay

To infect cells with pseudoviruses, HEK293T cells on the wells were co-transfected with 1,250 ng of ACE2 (Addgene plasmid #141185) and 1,250 ng of TMPRSS2 expression plasmids (Addgene plasmid #145843) in the six-well plate. After a transfection period of 48 h, HEK293T cells were harvested and seeded at $2 \times 10^4$ cells/well on 96-well black plates and incubated at 37°C and 5% $CO_2$ for 24 h. The following day, inhibition of montelukast to the entry of HEK293T/hACE2 cells was tested in three ways (1) the drug + pseudovirus was pretreated for 1 h at 37°C and then added to the cells, (2) the cell + drug was pretreated for 1 h at 37°C and then the pseudovirus was added, (3) the cell + pseudovirus was pretreated for 1 h at 37°C and then the drug was added. The infection rate by pseudoviruses was determined by measuring fluorescence intensity due to GFP reporter plasmids in the microplate reader. The cell viability in the same wells was determined by using CellTiter-Glo Luminescent Cell Viability Assay Kit (#G7571, Promega). Neutralization efficiency was calculated as relative fluorescence to the conditioned media collected from mock-transfected cells.

### Virus neutralization assay using xCELLigence MP RTCA

In the study, VERO E6 cell line (passage number: 17) was used. VERO E6 cells were cultured in DMEM with low glucose (DMEM/LOW GLUCOSE, HyClone, Cat # SH30021.01, lot # AF29484096) supplemented with a final concentration of 10% heat-inactivated FBS (HyClone, catalog # SV30160.03, lot # RE00000002) and 1% penicillin (10,000 units/mL) and streptomycin (10,000 units/mL) (HyClone, catalog # SV30010, lot # J190007). Sample stocks were diluted in DMEM low glucose supplemented with 2% FBS to make a concentration range. Neutralization assay was performed based on impedance using xCELLigence MP RTCA equipment (Agilent Technologies, CA). The impedance is expressed as arbitrary units called CI. VERO E6 cells were suspended in DMEM low glucose supplemented with 10% FBS and seeded into a disposable sterile 96-well E plate of the xCELLigence RTCA MP device at a final cell concentration of $2.5 \times 10^4$ cells per well. The instrument was placed in a $CO_2$ cell culture incubator during the experiment and was controlled by a cable connected to the control unit located outside the incubator. The cells on 96-well E plate were placed in the xCELLigence RTCA MP device and incubated for 24 h. After incubation, the experimental sample was divided into three groups. In the first group, the cells were incubated with montelukast at different concentrations (50, 35, 25, 12.5, and 6.25 μM) at 37°C for 1 h, with 5% $CO_2$ and then $3.1 \times 10^6$ PFU/mL SARS-CoV-2 was added to them. The second method consisted of incubating the cells with $3.1 \times 10^6$ PFU/mL SARS-CoV-2 at 37°C for 1 h with 5% $CO_2$, and then different concentrations of montelukast were added on the cells. In the last group, different montelukast concentrations and $3.1 \times 10^6$ PFU/mL SARS-CoV-2 were incubated at 37°C for 1 h with 5% $CO_2$ and then added to the cells. All samples were prepared in DMEM low glucose containing 2% FBS.

After all samples were introduced into the device, 130 h of sample collection was performed at 15-min intervals. At the end of the period, the experiment was terminated and the data obtained were analyzed using RTCA Software Pro software.

The electrical conductivity was converted into the unitless CI parameter by the xCELLigence MP device every 15 min. An increase in CI indicates cell viability/health, whereas a decrease indicates cell death/unhealth. It is expected that VERO E6 cells in the presence of the SARS-CoV-2 virus will demonstrate a decrease in CI values. The data shown in the figures are normalized according to the time point when the virus was added to the experiment.

The investigation of antiviral activity and pseudovirus and virus neutralization potential therapeutic agents against the live SARS-CoV-2 needs to be performed under biosafety level 3 conditions because of its high pathogenicity and infectivity.[60]

## SUPPLEMENTAL INFORMATION

Supplemental information can be found online at https://doi.org/10.1016/j.ymthe.2021.10.014.

## ACKNOWLEDGMENTS

This study was funded by Scientific Research Projects Commission of Bahçeşehir University; project number: BAU.BAP.2020.01. This study was also funded by the Scientific and Technological Research Council of Turkey (TÜBİTAK), within the program number of 18AG003. We would like to thank Néstor Santiago-Gonzalvo (Cytiva) for his helpful discussion and support with the Biacore experiments.

## AUTHOR CONTRIBUTIONS

S.D. designed and coordinated the project. S.D., A.A., S.C., L.O., I.T., E.E., A.O., A.O., E.A., S.B., and Y.Y. performed *in silico* simulations and analyses. T.A., M.D.O., and S.C. performed enzyme inhibition assays. B.K.B., H.U.O., and N.T. performed SPR experiments. A.K., Y.C., S.A., T.B.-O., S.T., H.D., M.G., Y.E.B., and S.I. performed pseudo virus neutralization assay experiments. M.S., S.T., and S.I. conducted virus neutralization experiments. The manuscript was prepared by S.D. with input from all the coauthors.

## DECLARATION OF INTERESTS

The authors declare no competing interests.

## REFERENCES

1. Huang, Y., Yang, C., Xu, X.F., Xu, W., and Liu, S.W. (2020). Structural and functional properties of SARS-CoV-2 spike protein: potential antivirus drug development for COVID-19. Acta Pharmacol. Sin. *41*, 1141–1149.
2. Ahn, D.G., Shin, H.J., Kim, M.H., Lee, S., Kim, H.S., Myoung, J., Kim, B.T., and Kim, S.J. (2020). Current status of epidemiology, diagnosis, therapeutics, and vaccines for novel coronavirus disease 2019 (COVID-19). J. Microbiol. Biotechnol. *30*, 313–324.
3. Shereen, M.A., Khan, S., Kazmi, A., Bashir, N., and Siddique, R. (2020). COVID-19 infection: origin, transmission, and characteristics of human coronaviruses. J. Adv. Res. *24*, 91–98.
4. Zhang, Y.Z., and Holmes, E.C. (2020). A genomic perspective on the origin and emergence of SARS-CoV-2. Cell *181*, 223–227.
5. Durdağı, S. (2020). Virtual drug repurposing study against SARS-CoV-2 TMPRSS2 target. Turkish J. Biol. *44*, 185–191.
6. Durdagi, S., Orhan, M.D., Aksoydan, B., Calis, S., Dogan, B., Sahin, K., Shahraki, A., Iyison, N.B., and Avsar, T. (2021). Screening of clinically approved and investigation drugs as potential inhibitors of SARS-CoV-2: a combined in silico and in vitro study. Mol. Inf. *40*, 2100062. https://doi.org/10.1002/minf.202100062.
7. Alyammahi, S.K., Abdin, S.M., Alhamad, D.W., Elgendy, S.M., Altell, A.T., and Omar, H.A. (2021). The dynamic association between COVID-19 and chronic disorders: an updated insight into prevalence, mechanisms and therapeutic modalities. Infect. Genet. Evol. *87*, 104647. https://doi.org/10.1016/j.meegid.2020.104647.
8. Chen, G., Wu, D., Guo, W., Cao, Y., Huang, D., Wang, H., Wang, T., Zhang, X., Chen, H., Yu, H., et al. (2020). Clinical and immunological features of severe and moderate coronavirus disease 2019. J. Clin. Invest. *130*, 2620–2629.
9. Huang, C., Wang, Y., Li, X., Ren, L., Zhao, J., Hu, Y., Zhang, L., Fan, G., Xu, J., Gu, X., et al. (2020). Clinical features of patients infected with 2019 novel coronavirus in Wuhan, China. Lancet *395*, 497–506.
10. Wan, S., Yi, Q., Fan, S., Lv, J., Zhang, X., Guo, L., Lang, C., Xiao, Q., Xiao, K., Yi, Z., et al. (2020). Characteristics of lymphocyte subsets and cytokines in peripheral blood of 123 hospitalized patients with 2019 novel coronavirus pneumonia (NCP). medRxiv. https://doi.org/10.1101/2020.02.10.20021832.
11. Diao, B., Wang, C., Tan, Y., Chen, X., Liu, Y., Ning, L., Chen, L., Li, M., Liu, Y., Wang, G., et al. (2020). Reduction and functional exhaustion of T cells in patients with coronavirus disease 2019 (COVID-19). Front. Immunol. *11*, 827. https://doi.org/10.3389/fimmu.2020.00827.
12. Williamson, E.J., Walker, A.J., Bhaskaran, K., Bacon, S., Bates, C., Morton, C.E., Curtis, H.J., Mehrkar, A., Evans, D., Inglesby, P., et al. (2020). Factors associated with COVID-19-related death using OpenSAFELY. Nature *584*, 430–436.
13. Oliver, B.G.G., Robinson, P., Peters, M., and Black, J. (2014). Viral infections and asthma: an inflammatory interface? Eur. Respir. J. *44*, 1666–1681.
14. Johnston, N.W., Johnston, S.L., Duncan, J.M., Greene, J.M., Kebadze, T., Keith, P.K., Roy, M., Waserman, S., and Sears, M.R. (2005). The September epidemic of asthma exacerbations in children: a search for etiology. J. Allergy Clin. Immunol. *115*, 132–138.
15. Zheng, X.-Y., Xu, Y.-J., Guan, W.-J., and Lin, L.-F. (2018). Regional, age and respiratory-secretion-specific prevalence of respiratory viruses associated with asthma exacerbation: a literature review. Arch. Virol. *163*, 845–853.
16. Gentile, D.A., Fireman, P., and Skoner, D.P. (2003). Elevations of local leukotriene C4 levels during viral upper respiratory tract infections. Ann. Allergy Asthma Immunol. *91*, 270–274.
17. Almerie, M.Q., and Kerrigan, D.D. (2020). The association between obesity and poor outcome after COVID-19 indicates a potential therapeutic role for montelukast. Med. Hypotheses. *143*, 109883. https://doi.org/10.1016/j.mehy.2020.109883.
18. Barré, J., Sabatier, J.M., and Annweiler, C. (2020). Montelukast drug may improve COVID-19 prognosis: a review of evidence. Front. Pharmacol. *11*, 1344. https://doi.org/10.3389/fphar.2020.01344.
19. Sanghai, N., and Tranmer, G.K. (2020). Taming the cytokine storm: repurposing montelukast for the attenuation and prophylaxis of severe COVID-19 symptoms. Drug Discov. Today *25*, 2076–2079.
20. Citron, F., Perelli, L., Deem, A.K., Genovese, G., and Viale, A. (2020). Leukotrienes, a potential target for Covid-19. Prostaglandins Leukot. Essent. Fat. Acids *161*, 102174. https://doi.org/10.1016/j.plefa.2020.102174.
21. Funk, C.D., and Ardakani, A. (2020). A novel strategy to mitigate the hyperinflammatory response to COVID-19 by targeting leukotrienes. Front. Pharmacol. *11*, 1214. https://doi.org/10.3389/fphar.2020.01214.
22. Reiss, T.F., Altman, L.C., Chervinsky, P., Bewtra, A., Stricker, W.E., Noonan, G.P., Kundu, S., and Zhang, J. (1996). Effects of montelukast (MK-0476), a new potent cysteinyl leukotriene (LTD4) receptor antagonist, in patients with chronic asthma. J. Allergy Clin. Immunol. *98*, 528–534.
23. Altman, L.C., Munk, Z., Seltzer, J., Noonan, N., Shingo, S., Zhang, J., and Reiss, T.F. (1998). A placebo-controlled, dose-ranging study of montelukast, a cysteinyl leukotriene-receptor antagonist. J. Allergy Clin. Immunol. *102*, 50–56.

24. Knorr, B., Holland, S., Schwartz, J., Douglas Rogers, J., and Reiss, T.F. (2001). Clinical pharmacology of montelukast. Clin. Exp. Allergy Rev. *1*, 254–260.

25. Ikram, S., Ahmad, J., and Durdagi, S. (2020). Screening of FDA approved drugs for finding potential inhibitors against Granzyme B as a potent drug-repurposing target. J. Mol. Graph. Model. *95*, 107642. https://doi.org/10.1016/j.jmgm.2019.107462.

26. Sahaboglu, A., Miranda, M., Canjuga, D., Avci-Adali, M., Savytska, N., Secer, E., Feria-Pliego, J.A., Kayık, G., and Durdagi, S. (2020). Drug repurposing studies of PARP inhibitors as a new therapy for inherited retinal degeneration. Cell. Mol. Life Sci. *77*, 2199–2216.

27. Dogan, B., and Durdagi, S. (2021). Drug re-positioning studies for novel HIV-1 inhibitors using binary QSAR models and multi-target-driven in silico studies. Mol. Inform. *40*, e2000012. https://doi.org/10.1002/minf.202000012.

28. Duarte, R.R.R., Copertino, D.C., Iñiguez, L.P., Marston, J.L., Bram, Y., Han, Y., Schwartz, R.E., Chen, S., Nixon, D.F., and Powell, T.R. (2021). Identifying FDA-approved drugs with multimodal properties against COVID-19 using a data-driven approach and a lung organoid model of SARS-CoV-2 entry. Mol. Med. *27*, 105. https://doi.org/10.1186/s10020-021-00356-6.

29. Bharath, B.R., Damle, H., Ganju, S., and Damle, L. (2020). In silico screening of known small molecules to bind ACE2 specific RBD on spike glycoprotein of SARS-CoV-2 for repurposing against COVID-19. F1000Research *9*, 663. https://doi.org/10.12688/f1000research.24143.1.

30. Jang, W.D., Jeon, S., Kim, S., and Lee, S.Y. (2021). Drugs repurposed for COVID-19 by virtual screening of 6,218 drugs and cell-based assay. Proc. Natl. Acad. Sci. U S A *118*. e2024302118. https://doi.org/10.1073/pnas.2024302118.

31. Nie, J., Li, Q., Wu, J., Zhao, C., Hao, H., Liu, H., Zhang, L., Nie, L., Qin, H., Wang, M., et al. (2020). Establishment and validation of a pseudovirus neutralization assay for SARS-CoV-2. Emerg. Microbes Infect. *9*, 680–686.

32. Durdagi, S., Dag, C., Dogan, B., Yigin, M., Avsar, T., Buyukdag, C., Erol, I., Ertem, B., Calis, S., Yildirim, G., et al. (2021). Near-physiological-temperature serial femtosecond X-ray crystallography reveals novel conformations of SARS-CoV-2 main protease active site for improved drug repurposing. Structure *S0969-2126*, 00257–264. https://doi.org/10.1016/j.str.2021.07.007.

33. Ramsay, R.R., Popovic-Nikolic, M.R., Nikolic, K., Uliassi, E., and Bolognesi, M.L. (2018). A perspective on multi-target drug discovery and design for complex diseases. Clin. Transl. Med. *7*, 3. https://doi.org/10.1186/s40169-017-0181-2.

34. Witkowski, P.T., Schuenadel, L., Wiethaus, J., Bourquain, D.R., Kurth, A., and Nitsche, A. (2010). Cellular impedance measurement as a new tool for poxvirus titration, antibody neutralization testing and evaluation of antiviral substances. Biochem. Biophys. Res. Commun. *401*, 37–41.

35. Charretier, C., Saulnier, A., Benair, L., Armanet, C., Bassard, I., Daulon, S., Bernigaud, B., Rodrigues de Sousa, E., Gonthier, C., Zorn, E., et al. (2018). Robust real-time cell analysis method for determining viral infectious titers during development of a viral vaccine production process. J. Virol. Methods *252*, 57–64.

36. Teng, Z., Kuang, X., Wang, J., and Zhang, X. (2013). Real-time cell analysis - a new method for dynamic, quantitative measurement of infectious viruses and antiserum neutralizing activity. J. Virol. Methods *193*, 364–370.

37. Fang, Y., Ye, P., Wang, X., Xu, X., and Reisen, W. (2011). Real-time monitoring of flavivirus induced cytopathogenesis using cell electric impedance technology. J. Virol. Methods *173*, 251–258.

38. Fidan, C., and Aydoğdu, A. (2020). As a potential treatment of COVID-19: montelukast. Med. Hypotheses. *142*, 109828. https://doi.org/10.1016/j.mehy.2020.109828.

39. Aigner, L., Pietrantonio, F., Bessa de Sousa, D.M., Michael, J., Schuster, D., Reitsamer, H.A., Zerbe, H., and Studnicka, M. (2020). The leukotriene receptor antagonist montelukast as a potential COVID-19 therapeutic. Front. Mol. Biosci. *7*, 610132. https://doi.org/10.3389/fmolb.2020.610132.

40. Farag, A., Wang, P., Ahmed, M., and Sadek, H. (2020). Identification of FDA approved drugs targeting COVID-19 virus by structure-based drug repositioning. ChemRxiv. https://doi.org/10.26434/chemrxiv.12003930.v3.

41. Wu, C., Liu, Y., Yang, Y., Zhang, P., Zhong, W., Wang, Y., Wang, Q., Xu, Y., Li, M., Li, X., et al. (2020). Analysis of therapeutic targets for SARS-CoV-2 and discovery of potential drugs by computational methods. Acta Pharm. Sin. B *10*, 766–788.

42. Copertino, D.C., Duarte, R.R.R., Powell, T.R., de Mulder Rougvie, M., and Nixon, D.F. (2021). Montelukast drug activity and potential against severe acute respiratory syndrome coronavirus 2 (SARS-CoV-2). J. Med. Virol. *93*, 187–189.

43. Neerukonda, S.N., Vassell, R., Herrup, R., Liu, S., Wang, T., Takeda, K., Yang, Y., Lin, T.L., Wang, W., and Weiss, C.D. (2021). Establishment of a well-characterized SARSCoV-2 lentiviral pseudovirus neutralization assay using 293T cells with stable expression of ACE2 and TMPRSS2. PLoS One *16*, e0248348. https://doi.org/10.1371/journal.pone.0248348.

44. Cifuentes-Muñoz, N., Darlix, J.L., and Tischler, N.D. (2010). Development of a lentiviral vector system to study the role of the Andes virus glycoproteins. Virus Res. *153*, 29–35.

45. Johnson, M.C., Lyddon, T.D., Suarez, R., Salcedo, B., LePique, M., Graham, M., Ricana, C., Robinson, C., and Ritter, D.G. (2020). Optimized pseudotyping conditions for the SARS-COV-2 spike glycoprotein. J. Virol. *94*. e01062–20. https://doi.org/10.1128/JVI.01062-20.

46. Xiong, H.L., Wu, Y.T., Cao, J.L., Yang, R., Liu, Y.X., Ma, J., Qiao, X.Y., Yao, X.Y., Zhang, B.H., Zhang, Y.L., et al. (2020). Robust neutralization assay based on SARS-CoV-2 S-protein-bearing vesicular stomatitis virus (VSV) pseudovirus and ACE2-overexpressing BHK21 cells. Emerg. Microbes Infect. *9*, 2105–2113.

47. Kumar, S., Singh, B., Kumari, P., Kumar, P.V., Agnihotri, G., Khan, S., Kant Beuria, T., Syed, G.H., and Dixit, A. (2021). Identification of multipotent drugs for COVID-19 therapeutics with the evaluation of their SARS-CoV2 inhibitory activity. Comput. Struct. Biotechnol. J. *19*, 1998–2017.

48. Shelley, J.C., Cholleti, A., Frye, L.L., Greenwood, J.R., Timlin, M.R., and Uchimaya, M. (2007). Epik: a software program for pKa prediction and protonation state generation for drug-like molecules. J. Comput. Aided. Mol. Des. *21*, 681–691.

49. Jacobson, M.P., Pincus, D.L., Rapp, C.S., Day, T.J.F., Honig, B., Shaw, D.E., and Friesner, R.A. (2004). A hierarchical approach to all-atom protein loop prediction. Proteins Struct. Funct. Genet. *55*, 351–367.

50. Friesner, R.A., Murphy, R.B., Repasky, M.P., Frye, L.L., Greenwood, J.R., Halgren, T.A., Sanschagrin, P.C., and Mainz, D.T. (2006). Extra precision glide: docking and scoring incorporating a model of hydrophobic enclosure for protein-ligand complexes. J. Med. Chem. *49*, 6177–6196.

51. Ali, A., and Vijayan, R. (2020). Dynamics of the ACE2–SARS-CoV-2/SARS-CoV spike protein interface reveal unique mechanisms. Sci. Rep. *10*, 14214. https://doi.org/10.1038/s41598-020-71188-3.

52. Zhu, K., Borrelli, K.W., Greenwood, J.R., Day, T., Abel, R., Farid, R.S., and Harder, E. (2014). Docking covalent inhibitors: a parameter free approach to pose prediction and scoring. J. Chem. Inf. Model. *54*, 1932–1940.

53. Bowers, K.J., Chow, E., Xu, H., Dror, R.O., Eastwood, M.P., Gregersen, B.A., Klepeis, J.L., Kolossvary, I., Moraes, M.A., Sacerdoti, F.D., et al. (2006). Scalable Algorithms for Molecular Dynamics Simulations on Commodity Clusters. In Proceedings of the ACM/IEEE Conference on Supercomputing (SC'06), Tampa, Florida, USA.

54. Nosé, S. (1984). A unified formulation of the constant temperature molecular dynamics methods. J. Chem. Phys. *81*, 511–519.

55. Hoover, W.G. (1985). Canonical dynamics: equilibrium phase-space distributions. Phys. Rev. A *31*, 1695–1697.

56. Martyna, G.J., Tobias, D.J., and Klein, M.L. (1994). Constant pressure molecular dynamics algorithms. J. Chem. Phys. *101*, 4177–4189.

57. Essmann, U., Perera, L., Berkowitz, M.L., Darden, T., Lee, H., and Pedersen, L.G. (1995). A smooth particle mesh Ewald method. J. Chem. Phys. *103*, 8577–8593.

58. Harder, E., Damm, W., Maple, J., Wu, C., Reboul, M., Xiang, J.Y., Wang, L., Lupyan, D., Dahlgren, M.K., Knight, J.L., et al. (2016). OPLS3: a force field providing broad coverage of drug-like small molecules and proteins. J. Chem. Theor. Comput. *12*, 281–296.

59. Grehan, K., Ferrara, F., and Temperton, N. (2015). An optimised method for the production of MERS-CoV spike expressing viral pseudotypes. MethodsX *2*, 379–384.

60. Millet, J.K., Tang, T., Nathan, L., Jaimes, J.A., Hsu, H.L., Daniel, S., and Whittaker, G.R. (2019). Production of pseudotyped particles to study highly pathogenic coronaviruses in a biosafety level 2 setting. J. Vis. Exp. *145*. https://doi.org/10.3791/59010.